actuators

MDPI

Article

Design and Analysis of an Adaptive Cable-Driven Manipulator Capable of Actively Transitioning between Two-Point Clamping and Envelope Grasping

Huiling Wei [1], Jin Liu [2], Qinghua Lu [1,*], Weilin Chen [1], Lufeng Luo [1] and Chengbin Liang [1]

[1] School of Mechatronic Engineering and Automation, Foshan University, Foshan 528000, China; weihuiling2007@fosu.edu.cn (H.W.); weilin.chen@fosu.edu.cn (W.C.); luolufeng@fosu.edu.cn (L.L.); 2112202053@stu.fosu.edu.cn (C.L.)

[2] College of Intelligent Manufacturing, Foshan Polytechnic, Foshan 528137, China; jin12345678@fspt.edu.cn

* Correspondence: qhlu@fosu.edu.cn

Abstract: Actively transitioning between clamping and grasping is a challenging problem for most manipulators with limited degrees of freedom. To overcome this problem, a cable-driven rigid–flexible combined manipulator capable of actively transitioning between clamping and grasping is proposed in this paper, which has a certain adaptability and compliance to achieve adaptive operation. First, the cable-driven unit and compliant unit of the cable-driven rigid–flexible combined manipulator are designed. Then, the sensitivity of the mechanism parameters is analyzed using the Monte Carlo method, and then the structure of the cable-driven rigid–flexible combined manipulator is optimized. After that, the force on the finger in two-point clamping mode is modelled using Newton's second law. Furthermore, the input–output relationship modelling of the finger in envelope grasping mode is deeply analyzed using the principle of energy conservation. Finally, the stable grasping performance of the cable-driven rigid–flexible combined manipulator is verified using numerical simulation and physical prototype tests. The results show that the cable-driven rigid–flexible combined manipulator has good adaptability and compliance, which verifies the effectiveness and rationality of the design and modelling.

Keywords: cable-driven manipulator; modeling; sensitivity analysis; design optimization; performance evaluation

check for updates

Citation: Wei, H.; Liu, J.; Lu, Q.; Chen, W.; Luo, L.; Liang, C. Design and Analysis of an Adaptive Cable-Driven Manipulator Capable of Actively Transitioning between Two-Point Clamping and Envelope Grasping. *Actuators* **2023**, *12*, 461. https://doi.org/10.3390/act12120461

Academic Editor: Ioan Ursu

Received: 27 September 2023
Revised: 23 November 2023
Accepted: 9 December 2023
Published: 11 December 2023

Copyright: © 2023 by the authors. Licensee MDPI, Basel, Switzerland. This article is an open access article distributed under the terms and conditions of the Creative Commons Attribution (CC BY) license (https://creativecommons.org/licenses/by/4.0/).

1. Introduction

There are still certain challenges for adaptive stable grasping on targets such as vulnerable bodies and irregular parts. The key to solving this problem is to design the manipulator with certain adaptability and flexibility for multimode active switching. Therefore, this work focuses on researching a manipulator that can achieve active switching between two-point clamping and envelope grasping.

The advantages of cable-driven parallel mechanisms are high flexibility, low motion inertia, reconfigurability, and quick response times. A certain degree of adaptability and compliance for the grasped movement is provided by the driving cable's flexible elasticity [1], which can improve the anti-damage coupling ability between the grasped target and the mechanism and enable a better dynamic interaction between the target and the mechanism [2]. This type of mechanism has been successfully applied in the fields of material handling, logistics and transportation, agricultural monitoring, disaster relief, limb rehabilitation, and high-speed cameras [3–8]. The cable-driven rigid–flexible combined manipulator is composed of a cable-driven system and a compliant mechanism, which has a certain flexibility and sufficient grasping force, overcoming the problems of insufficient flexibility in traditional rigid manipulators and insufficient grasping force in pure soft robots. It has broad application prospects in intelligent grasping tasks.

As one of the important end-effectors of robots, the manipulator is the key component in direct contact with the grasped target [9] and determines the operating performance. Therefore, the design of manipulator is very important. Babin et al. [10] conducted a detailed literature review on the design of robotic mechanical grippers. Babin indicated that no single gripper can perform every possible grasping or manipulation task. So, many specialized manipulators specifically designed for specific tasks are used in different fields. And for the rigid–flexible combined cable-driven parallel robot studied in this article, Zhang et al. [11] provided a comprehensive summary of its theories and developments. His review showed that the performance and practicality of the rigid–flexible combined cable-driven parallel robot can be improved by the combination of rigid chains, parallel cables, and passive tensioning elements. This idea provides a new approach for the configuration design of high-performance cable-driven parallel robots.

So far, some researchers have conducted in-depth research on the structural design, mechanical analysis of cable-driven manipulators. Ma et al. [12] proposed a multimode gripper with asymmetric hand design, which consists of a dexterous cable-driven index finger and a modular thumb with varying degrees of passive compliance. The thumb is not actuated, so the gripper is unable to complete symmetrical operation. Bircher et al. [13] designed a grasp–reposition–reorient gripper to address the challenging problem of repositioning objects while maintaining stable grasp in robotic manipulation. This study provided a new approach for the design of multifunctional grippers without using sensors. Firouzeh et al. [14] presented a design of tendon-driven robotic origami, which possessed the features self-adaptability and inherent softness due to its redundant and underactuated degrees of freedom. This research also verified the task versatility of the manipulator in soft and stiff modes by specifying model-based joint stiffnesses for performing different grasping modes. Based on this research, some grippers with soft and stiff modes can be designed. Dong et al. [15] proposed a fingertip optimization design model to evaluate the best fingertip shape and determine the size range of objects that could be steadily grasped by fingertips. However, the relationship between the geometric parameters and grasping stability was not established. Leddy et al. [16] proposed a constraint optimization framework, to evaluate the post contact stability of a single degree of actuation of an underactuated precision manipulator. Kim et al. [17] proposed a three-finger adaptive manipulator with five degrees of freedom and the ability actively transition between precise parallel clamping and compliant clamping. Hussain [18] presented the use of interpenetrating composite materials and a prism topology based on mathematical control with a minimum surface to create a soft gripper with the required stiffness. Min et al. [19] presented a novel design of an anthropomorphic robotic hand driven by parallel cables with a single motor that mimicked the muscle antagonism of the human hand. Zhang et al. [20] presented a new design scheme for an actuator with a zigzag cable routing mode, which was proposed to realize the transition from 2D bending to 3D motion. Xiong et al. [21] presented an adaptive multikernel dictionary learning method to analyze the characteristics of grasping force and the force coupling between multiple fingers, which improved the performance of robotic grasping state recognition. This work effectively overcomes the force correlation between multiple fingers and the individual tactile sensors. Zhang et al. [22] proposed a six-step approach to simulate the grasp for a versatile vacuum manipulator, which evaluated the grasp quality using a gripping attention convolutional neural network. This study effectively solved the problem of flexible grasping of unknown objects in unstructured environments.

Modeling and analysis on cable-driven manipulators were carried out in the above studies; however, the above research has not adequately achieved the function of multi grab mode switching, or the integrated design of adaptability and compliance. Although the relationship between the design parameters and the output force has not been established in some of the literature, there is a lack of sensitivity analysis of the design parameters, which is necessary for optimizing design. Therefore, in this paper, a mathematical model between the design parameters and the output force is established by modeling and sensitivity analysis of the design parameters of a cable-driven rigid–flexible combined manipulator.

To realize the adaptability and compliance of the manipulator, the research object in this paper is the cable-driven rigid–flexible combined manipulator, as shown in Figure 1. Its cable-driven unit and compliant unit are designed. The variance in parameters in sensitivity analysis is calculated using the Monte Carlo method. The force model of the cable-driven rigid–flexible combined manipulator in two-point clamping mode is established, and the input–output relationship model of the finger in envelope grasping mode is discussed in depth. Finally, to verify the grasp performance of the cable-driven rigid–flexible combined manipulator, grasp performance comparison tests are carried out in two-point clamping mode and envelope grasping mode.

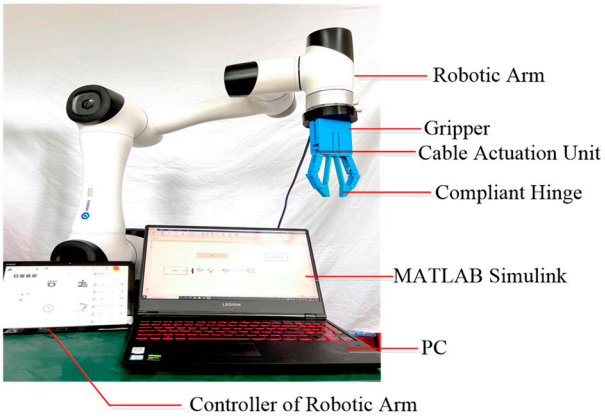

Figure 1. Schematic diagram of a cable-driven rigid–flexible combined manipulator.

2. Design of the Cable-Driven Manipulator

The characteristic of this study is to combine a compliant mechanism with a cable-driven system to solve the problem of automatic mode switching. A cable-driven system is adopted to achieve a certain adaptive grasping function, and a compliant mechanism is used to achieve a compliant fit between the fingers and the grasped target.

The cable-driven rigid–flexible combined manipulator is mainly composed of three parts: a cable-driven system, a compliant unit, and a rigid structure. The cable-driven system consists of cables, pulleys, motors, and hinge points. The flexibility of the cables can improve the adaptability of the manipulator. The compliant unit is mainly composed of compliant fingertips, compliant hinges, and compliant beams, which realizes the adaptive fit between the manipulator and the grasped target and enhances the compliance of the manipulator. The design of the cable-driven rigid–flexible combined manipulator is discussed in this section.

2.1. Design of the Cable Actuation Units

To endow the manipulator with certain adaptability and compliance features, the use of a cable-driven system to transmit power and motion is proposed. The design of the cable path for the cable-driven rigid–flexible combined manipulator in different clamping modes is shown in Figure 2.

The design of the cable path for the manipulator in two-point clamping mode and envelope grasping mode is shown in Figure 2a. As shown in Figure 2a, the cable paths are symmetrically distributed, and cables 1 and 2 are driven by motor 1. Each cable is driven by three two-way pulley blocks. Each cable is connected to the rigid structure through hinges 1 and 2. Due to the unidirectional force of the cable, the mechanical fingers of the cable-driven rigid–flexible combined manipulator are only subjected to cable tension, so the manipulator passively returns to the initial position. To realize the automatic reset of the cable-driven rigid–flexible combined manipulator, the design includes the placement of torsion tension spring 1 at the joint to provide stretching force to ensure the automatic reset of the manipulator.

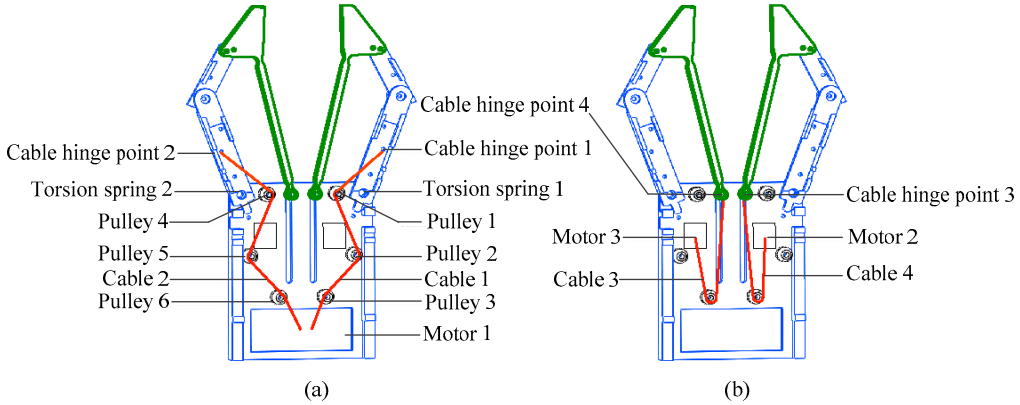

Figure 2. Schematic diagram of the cable path. (**a**) Two-point and envelope clamping; (**b**) Twist grasp mode.

The cable path design of the manipulator in twisting mode is shown in Figure 2b. As shown in Figure 2b, the cable path is still a left–right symmetrical design, and the two cables are driven by different motors. Each cable is fastened to the flexible connection unit with hinges 3 and 4. In the process of grasping, the object is first grasped in two-point clamping mode as driven by motor 1. On this basis, motors 2 and 3 are controlled to twist the grasped object and the flexible mechanism, respectively, under the action of the surface friction force.

2.2. Design of the Compliant Units

To achieve the stable grasping of fragile and specially shaped parts, the manipulator is required to have a certain adaptive grasping ability. In this paper, a compliant unit is designed to realize the adaptive fit between the manipulator and the grasped target to achieve stable grasping, as shown in Figure 3. It is a circular arc compliant hinge, which has a kind of kinematic pair structure that can generate relative motion between the flexible beam, the fingertip, and the base [23]. Compared with rigid hinges, compliant hinges have the advantages of being simple to manufacture and assembly-free and are widely used in compliant mechanisms. To increase the friction force of the fingertip, a gear-shaped fingertip contact surface is designed on the flexible fingertip to improve the stable grasping ability of the manipulator.

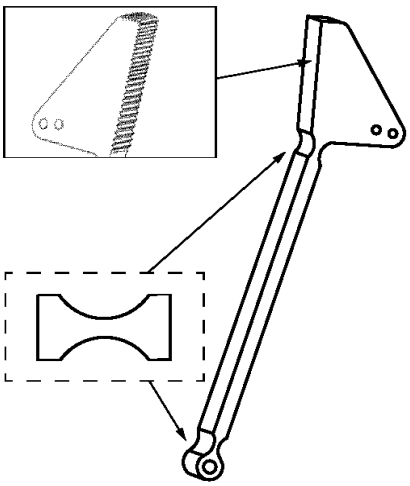

Figure 3. Schematic diagram of compliant unit.

3. Modeling under Different Poses

3.1. Force Modeling of Two-Point Clamping

Because the manipulator is driven by cables, it is necessary to establish a mathematical relationship between the cable tension and the cable stretch variables. Since the manipulator is a left–right symmetrical mechanism, it is only necessary to take half of it as the research object for mechanical analysis. In this section, the right half of the manipulator is selected for grasping force analysis. The position of the manipulator in any working state is shown in Figure 4, where A_1 is cable hinge point 1, B_1 is pulley 1, J_1 is torsion spring joint 1, L_1 is the distance between B_1 and J_1, L_2 is the distance between A_1 and J_1, and θ_1 is the angle between A_1J_1 and the horizontal line.

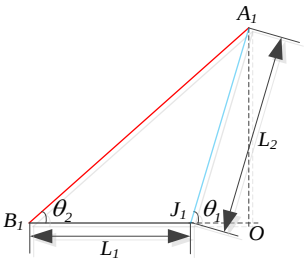

Figure 4. Geometric diagram of the cable length.

According to the geometric relationship shown in Figure 4, the cable stretch is expressed by:

$$\Delta L_{A_1B_1} = L_{\text{initial}} - L_{A_1B_1} = (L_1 + L_2) - \sqrt{(L_2\cos\theta_1 + L_1)^2 + (L_2\sin\theta_1)^2} \tag{1}$$

where L_{initial} is the distance between D and E at the initial limit position.

Assuming there is no interaction force between the finger and the object or environment, ignoring cable friction, the torque at joint J_1 is expressed by:

$$\boldsymbol{M}_{B_1} = \boldsymbol{M}_d - \boldsymbol{M}_{t1} = \boldsymbol{T}_1 R_1 - K\Delta\theta_1 \tag{2}$$

where $\boldsymbol{M}_d$ is the driving torque, $\boldsymbol{M}_{t1}$ is the deformation torque of the torsion spring, $\boldsymbol{T}_1$ is the cable tension, R_1 is the distance from joint J_1 to the cable, K is the stiffness of the torsion spring, and $\Delta\theta_1$ is the deformation of the torsion spring at joint J_1.

When the cable-driven rigid–flexible combined manipulator is in two-point clamping mode, the contact surface of the two flexible fingertips is parallel to the gripper symmetry axis, as shown in Figure 5, where xoy is the reference coordinate system, J_1 is the hinge point of the base and the first rigid knuckle, J_2 is the hinge point of the first rigid knuckle and the second rigid knuckle, J_3 is the hinge point of the second rigid knuckle and the flexible fingertip, P_1 is the hinge point between the proximal end of the flexible beam (the end closer to the base is set as the proximal end) and the base, P_2 is the hinge center point at the distal end of the flexible beam, and P_5 is the contact point between the flexible fingertip and the grasped target.

According to the coordinate system and geometric relationship, the coordinates of each point are expressed as follows:

$$J_1 = (x_{J_1}, y_{J_1}) = (d_1 + d_2, 0) \tag{3}$$

$$J_2 = (x_{J_2}, y_{J_2}) = (d_1 + d_2 + l_1\cos\theta_1, l_1\sin\theta_1) \tag{4}$$

$$J_3 = (x_{J_3}, y_{J_3}) = \left(d_0 + d, \sqrt{l_4^2 - (d_0 - d_1)^2}\right) \tag{5}$$

$$P_1 = (x_{P_1}, y_{P_1}) = (d_1, 0) \tag{6}$$

$$P_2 = (x_{P_2}, y_{P_2}) = \left(d_0, \sqrt{l_4^2 - (d_0 - d_1)^2}\right) \tag{7}$$

$$P_5 = (x_{P_5}, y_{P_5}) = \left(d_0, l_3 + \sqrt{l_4^2 - (d_0 - d_1)^2}\right) \tag{8}$$

where l_1 is the length of the first rigid knuckle, l_3 is the distance between the contact point and the center point of the hinge at the distal end of the flexible beam, l_4 is the length of the flexible beam, d_0 is the radius of the grasped target, d_1 is the horizontal distance from P_1 to the axis symmetry, d_2 is the horizontal distance between P_1 and J_1, and d is the horizontal distance between P_2 and J_3.

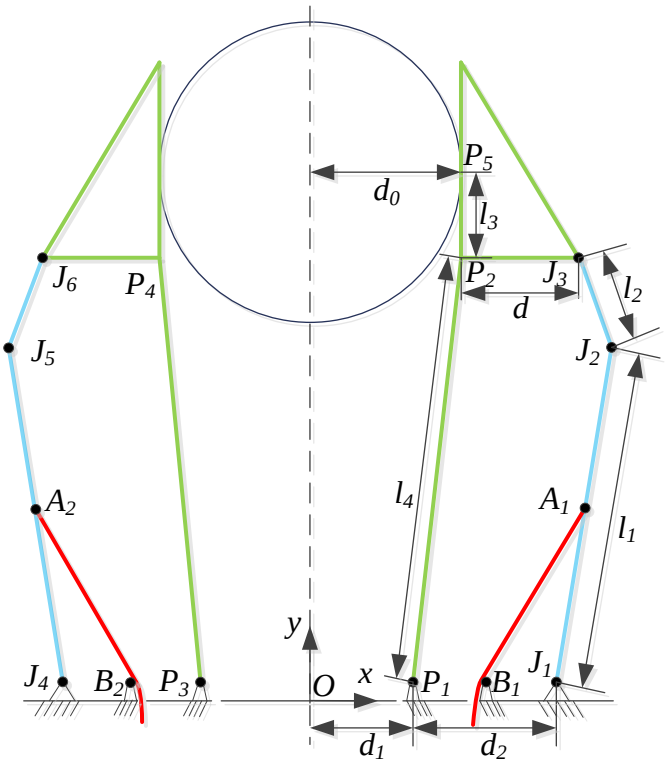

Figure 5. Schematic diagram of the two-point clamping mode. The green line represents the compliant unit; The blue line represents a rigid body; The red line represents the cable.

To construct a static model of the manipulator in two-point clamping mode, the force on each part of the finger is determined, as shown in Figure 6. This study assumes small deformations for flexible materials and ignores deformations for rigid materials.

Since the grasped target is the research object, as shown in Figure 6a, it is subjected to the pressure and friction of the flexible fingertips, as well as its own gravity. When the grasped target is quasistatic, according to the static force balance relationship, the static equilibrium is expressed by:

$$\boldsymbol{F}_{N1} + \boldsymbol{F}_{N2} = 0 \tag{9}$$

$$\boldsymbol{f}_1 + \boldsymbol{f}_2 = \boldsymbol{G} \tag{10}$$

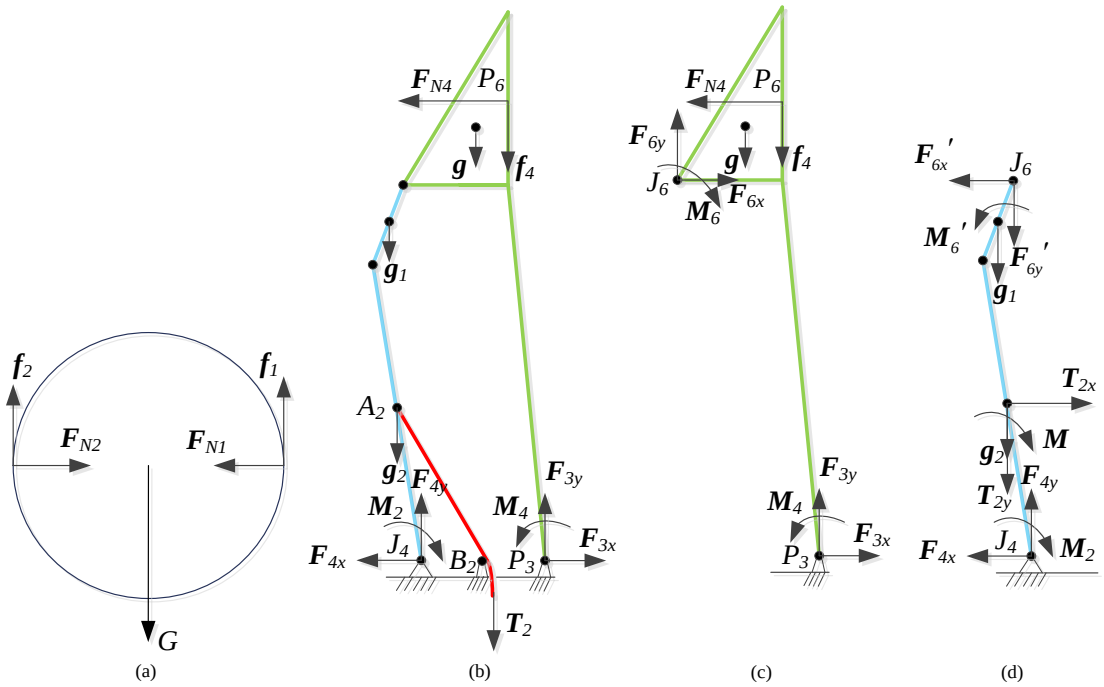

Figure 6. Force analysis of the finger in two-point clamping mode. (**a**) The grasping target; (**b**) The left side of gripper; (**c**) The compliant hinge unit; (**d**) The rigid knuckle. The green line represents the compliant unit; The blue line represents a rigid body; The red line represents the cable.

Since the manipulator is a left–right symmetrical structure, the left side was selected as the research object, and the force analysis is shown in Figure 6b. According to the equilibrium theory, the following expressions can be obtained:

$$\begin{aligned} \sum F_x = 0 \Rightarrow F_{3x} - F_{4x} - F_{N4} = 0 \\ \sum F_y = 0 \Rightarrow F_{3y} + F_{4y} - f_4 - T_2 - g - g_1 - g_2 = 0 \end{aligned} \tag{11}$$

$$\begin{aligned} M_2 - M_4 - F_{N4}\left(l_3 + \sqrt{l_4^2 - (d_0 - d_1)^2}\right) + f_4(d_2 + d_1 - d_0 - L_1) + \cdots \\ + \tfrac{1}{2}(l_2 g_1 \cos\theta_3 - l_1 g_2 \cos\theta_2) - g\left(\tfrac{1}{3}d + L_1 + d_0 - d_1 - d_2\right) = 0 \end{aligned} \tag{12}$$

where g is the gravity of the compliant hinge unit, g_1 is the gravity of the first rigid knuckle, g_2 is the gravity of the second rigid knuckle.

The compliant hinge unit is then selected as the research object, and the corresponding force analysis is shown in Figure 6c. According to the equilibrium theory, the following expressions can be obtained:

$$\begin{aligned} \sum F_x = 0 \Rightarrow F_{3x} + F_{6x} - F_{N4} = 0 \\ \sum F_y = 0 \Rightarrow F_{3y} + F_{6y} - f_4 - g = 0 \end{aligned} \tag{13}$$

$$M_6 - M_4 - F_{N4}\left(l_3 + \sqrt{l_4^2 - (d_0 - d_1)^2}\right) - f_4(d_0 - d_1) - g\left(\frac{1}{3}d + d_0 - d_1\right) = 0 \tag{14}$$

The rigid knuckles are then selected as the research object, and force analysis is carried out, as shown in Figure 6d. According to the static force balance relationship, the following expressions can be obtained:

$$\begin{aligned} \sum F_x = 0 \Rightarrow T_{2x} - F_{6x}{}' - F_{4x} = 0 \\ \sum F_y = 0 \Rightarrow F_{4y} - F_{6y}{}' - T_{2y} - g_1 - g_2 = 0 \end{aligned} \tag{15}$$

$$\boldsymbol{M} + \boldsymbol{M}_2 + \frac{1}{2} l_2 \boldsymbol{g}_1 \cos\theta_3 - \boldsymbol{M}_6{}' - \frac{1}{2} l_1 \boldsymbol{g}_2 \cos\theta_2 = 0 \tag{16}$$

By combining Equations (9)–(16), the mathematical model between the clamping force and the cable tension is obtained as follows:

$$\begin{aligned} \boldsymbol{F}_{N4} = \boldsymbol{T}_2 \frac{(d_2 \sin\theta_2 - d_2 + 2L_1)}{2\left(l_3 + \sqrt{l_4^2 - (d_0 - d_1)^2}\right)} + \frac{(l_2 \boldsymbol{g}_1 \cos\theta_3 - l_1 \boldsymbol{g}_2 \cos\theta_2)}{12\left(l_3 + \sqrt{l_4^2 - (d_0 - d_1)^2}\right)} - \\ \frac{\boldsymbol{G}(d_0 - d_1)}{2\left(l_3 + \sqrt{l_4^2 - (d_0 - d_1)^2}\right)} - \frac{\boldsymbol{g}(3d_0 - 3d_1 + d)}{3\left(l_3 + \sqrt{l_4^2 - (d_0 - d_1)^2}\right)} \end{aligned} \tag{17}$$

where θ_2 is the angle between the cable and the horizontal line.

3.2. Input–Output Relationship Modeling in Envelope Grasping Mode

When the cable-driven rigid–flexible combined manipulator is in envelope grasping mode, the contact form between the manipulator and the grasped target is surface contact, as shown in Figure 7. The force between the flexible beam and the grasped target originates from a distributed load, and it is difficult to directly establish the relationship between the distributed load and cable tension. Therefore, in this paper, the input–output relationship is established from the perspective of function transformation.

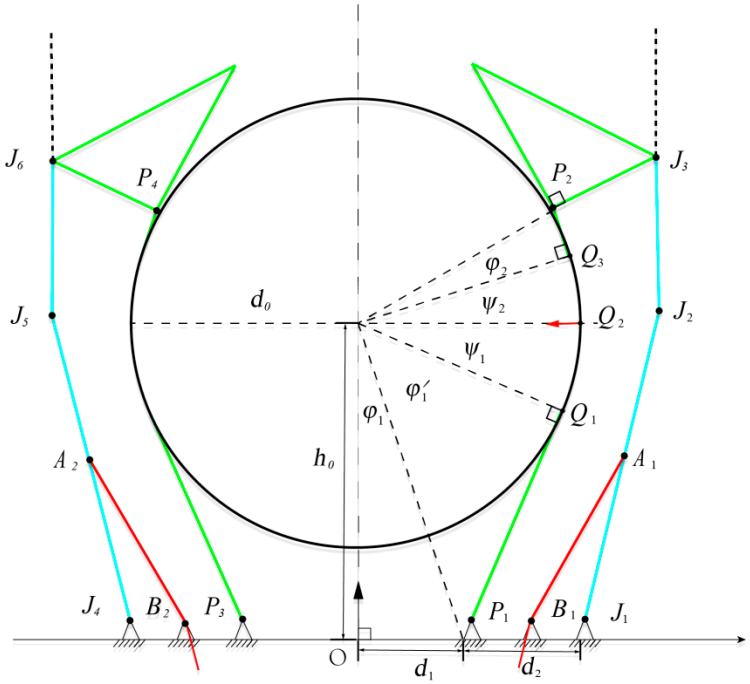

Figure 7. Schematic diagram of the envelope grasping mode. The green line represents the compliant unit; The blue line represents a rigid body; The red line represents the cable.

Since the thickness of the fingertip is much larger than that of the flexible beam, the deformation of the fingertip can be ignored. The bending deformation of flexible beams occurs during envelope grasping, so the influence of beam deformation needs to be considered when modeling. The contact surface during envelope grasping is a flexible beam element, and the input–output relationship is modelled using the principle of energy conservation during the grasping process. Based on previous research on compliant mechanisms [24], in order to reduce the nonlinearity and strong coupling of the model, the corresponding assumptions are as follows: (1) only the axial tensile and bending effects of the flexible beam are considered, and the torsional effect is not considered; (2) this study does not involve the shear deformation of flexible hinges; the flexible beam satisfies the

small deformation assumption of the Euler–Bernoulli beam; and (3) the contact force is assumed to be the concentrated force of the flexible beam.

The manipulator was selected as the research object, and energy conservation analysis was carried out. The input of the manipulator is the work performed by the cable tension, and the output is converted into four energy components: one is the gravitational potential energy that keeps the grasped target stationary, the second is the elastic potential energy of the torsion spring, the third is the elastic strain energy of the two compliant hinges, and the fourth is the elastic potential energy of the flexible beam. Therefore, the following expression can be obtained:

$$W = U_G + U_{t1} + 2U_c + U_b \tag{18}$$

where W is the input, U_G is the gravitational potential energy of the grasped target, U_{t1} is the elastic potential energy of the torsion spring, U_c is the elastic strain energy of the compliant hinge, and U_b is the elastic potential energy of the flexible beam.

Since the manipulator is symmetrical from left to right, the left side is selected as the analysis object. According to Figure 6, the input can be expressed as:

$$W = \boldsymbol{T}_2 \Delta L_{AB} \tag{19}$$

where ΔL_{AB} is the cable stretch, $\boldsymbol{T}_2$ is the cable tension.

According to Figure 6, the gravitational potential energy is expressed as:

$$U_G = \boldsymbol{G} h_0 \tag{20}$$

where $\boldsymbol{G}$ is the gravity of the grasped target, h_0 is the height of the center of gravity of the grasped target.

The elastic potential energy of the torsion spring can be expressed as:

$$U_{t1} = \frac{1}{2} K (\Delta\theta)^2 \tag{21}$$

where K is the stiffness of the torsion spring and $\Delta\theta$ is the deformation of the torsion spring.

The compliant hinge is equivalent to a cantilever beam with three nodes, as shown in Figure 8. The compliant hinges are modelled and analyzed using small-displacement Euler–Bernoulli beams, which are subjected to bending moment effects from forces and moments as well as axial loads.

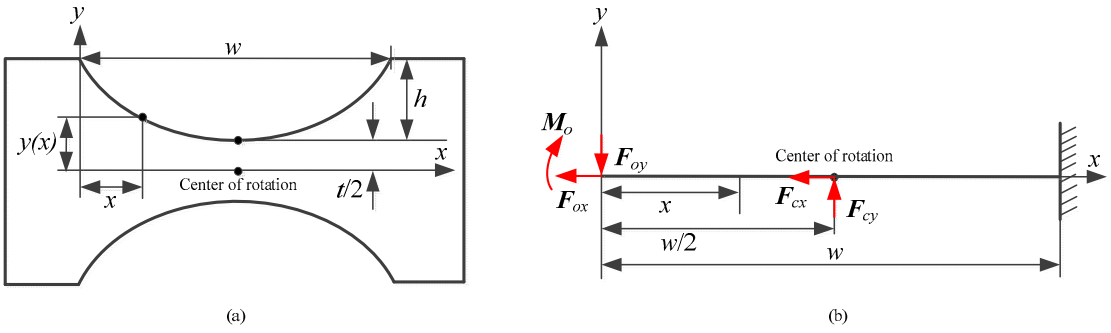

Figure 8. Compliant hinge assumed to be a small-displacement Euler–Bernoulli beam. (**a**) Schematic diagram of the compliant hinge; (**b**) Load Analysis of the compliant hinge.

According to Castigliano's second theorem, the elastic strain energy of the compliant hinge is expressed as:

$$\boldsymbol{U}_c = \frac{1}{2}\int_0^w \frac{\left[\boldsymbol{M}_o + (w-x)\boldsymbol{F}_{oy}\right]^2}{E\boldsymbol{I}(x)}\mathrm{d}x + \frac{1}{2}\int_0^w \frac{{\boldsymbol{F}_{ox}}^2}{EA(x)}\mathrm{d}x \tag{22}$$

where $\boldsymbol{M}_o$ is the bending moment, w is the length of the circular arc notch of the compliant hinge, $\boldsymbol{F}_{oy}$ is the vertical force, E is Young's modulus, $\boldsymbol{I}(x)$ is the flexure cross-sectional moment of inertia, $A(x)$ is the flexure cross-sectional area, and $\boldsymbol{F}_{ox}$ is the normal force.

According to previous research [25], the contour equation of compliant hinges is:

$$y(x) = \begin{cases} -\frac{6.664}{w^2}x^3 - \frac{6.436}{w}x^2 - 2.186x + 0.057w, & x \in \left(0, \frac{w}{2}\right) \\ t, & x = \frac{w}{2} \\ \frac{4.144}{w^2}x^3 - \frac{6.748}{w}x^2 + 2.302x + 0.054w, & x \in \left(\frac{w}{2}, w\right) \end{cases} \tag{23}$$

The moment of inertia and cross-sectional area of the arc-shaped compliant hinge cross-section are expressed as follows:

$$\begin{array}{l} I(x) = \frac{a[y(x)]^3}{12} \\ A(x) = ay(x) \end{array} \tag{24}$$

where a is the width of the arc compliant hinge.

Both ends of the flexible beam are arc compliant hinges, which are equivalent to simply supported beams. The corresponding force analysis is shown in Figure 9. The flexible beam is subjected to bending and axial tension under the action of force, and its elastic potential energy is expressed as:

$$U_b = \frac{1}{2}\mathrm{K}_x(\Delta x)^2 + \frac{1}{2}\mathrm{K}_y{\Delta_\mathrm{k}}^2 \tag{25}$$

where K_x is the axial elasticity coefficient, K_y is the radial elastic coefficient, Δ_k is the deflection of the flexible beam, and Δx is the stretch of the flexible beam.

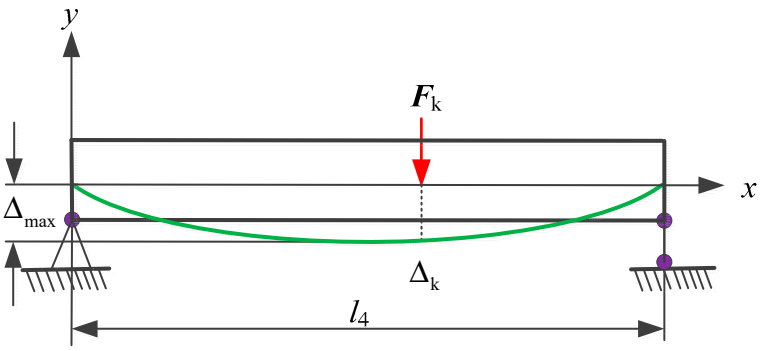

Figure 9. Schematic diagram of the force analysis of the flexible beam. The purple circles are hinge points.

According to Castigliano's second theorem, the relationship between load and displacement can also be written as [25]:

$$\boldsymbol{X} = \boldsymbol{C}\boldsymbol{F}_\mathrm{k} \tag{26}$$

where $\boldsymbol{C}$ is the flexible matrix.

The flexible beam is elastically deformed, and its deformation relationship is expressed as:

$$\Delta_\mathrm{k} = \frac{1}{2}\sqrt{(\Delta x)^2 + 2\Delta x l_4} \tag{27}$$

Because $\boldsymbol{K} = \frac{1}{\boldsymbol{C}}$, by substituting Equation (26) into Equation (25), Equation (25) can be reformulated as:

$$U_b = \frac{1}{2\boldsymbol{C}_x}(\Delta x)^2 + \frac{1}{2\boldsymbol{C}_y}(\Delta_\mathrm{k})^2 \tag{28}$$

3.3. Simulation Analysis of the Model

To verify the correctness and effectiveness of the static model, the output forces in two clamping modes were analyzed using RecurDyn. The setting of some simulation boundary conditions was converted according to Equations (19)–(28), including spring parameters, the geometric parameters, and the physical parameters of the compliant hinge. A torsion spring was installed at the hinge between the base and root finger, as well as between the root and end fingers, to ensure that the manipulator could return to its initial position. The torsion spring stiffness was K = 0.8 N·mm/(°). The motion duration was set to 5 s, with a reverse opening motion for the first second and a positive closing motion with a given torque for the second. Six groups of calculation examples were set up in different clamping modes to calculate the average value of the output force to compare the theoretical value with the simulation value.

The cable-driven torque was set to 114 N·mm. The simulation and theoretical results of the output force under different modes are shown in Figure 10. It can be seen from the figure that the maximum relative error is 5.78% for two-point clamping and 6.98% for envelope grasping. That is, the relative error between the theoretical value and the simulation value of the output force in envelope grasping and two-point clamping is within 7%. Due to the use of torque-equivalent cable force in numerical simulation, some errors occurred, but the relative error met engineering application requirements. In two-point clamping mode, the relative error between the simulated value and the theoretical value of the output force decreased gradually with increasing grasped target radius. In envelope grasping mode, the relative error did not change much with increasing grasped target radius.

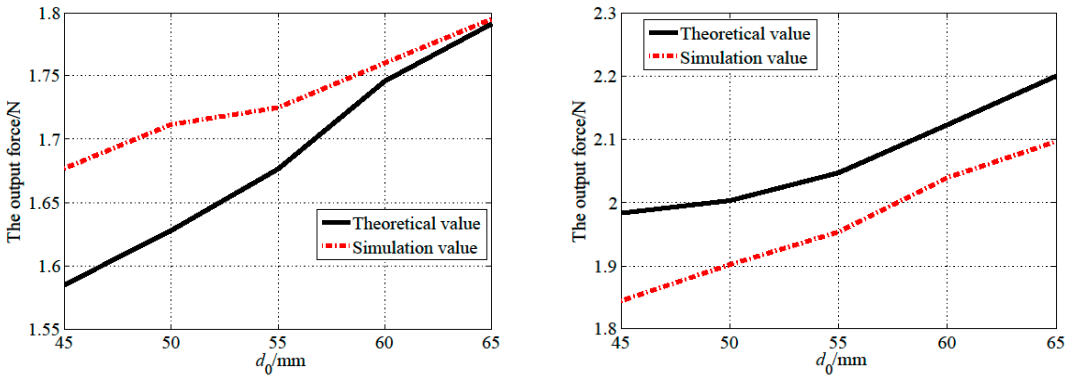

Figure 10. Output force simulation results in two modes with a torque of 114 N·mm. (**a**) Two-point clamping mode. (**b**) Envelope clamping mode.

The simulation and theoretical results of the output force in different modes when setting the cable-driven torque to 171 N·mm are shown in Figure 11. It can be seen from the figure that the maximum relative error is 3.25% for two-point clamping and 1.19% for envelope grasping. That is, the relative error between the theoretical value and the simulation value of the output force between envelope grasping and two-point clamping is within 5%, which meets engineering application requirements. In two-point clamping mode, the relative error between the simulation value and the theoretical value of the output force first decreases and then increases with increasing grasped target radius. In envelope grasping mode, the variation trend of the relative error is the same as that of two-point clamping with increasing grasped target radius. The reasons for the output force errors are multifaceted. Neglecting the friction of the cable-driven systems during theoretical modeling is one of the possible reasons for errors, and the elastic deformation of twisted springs and flexible materials may also have introduced errors.

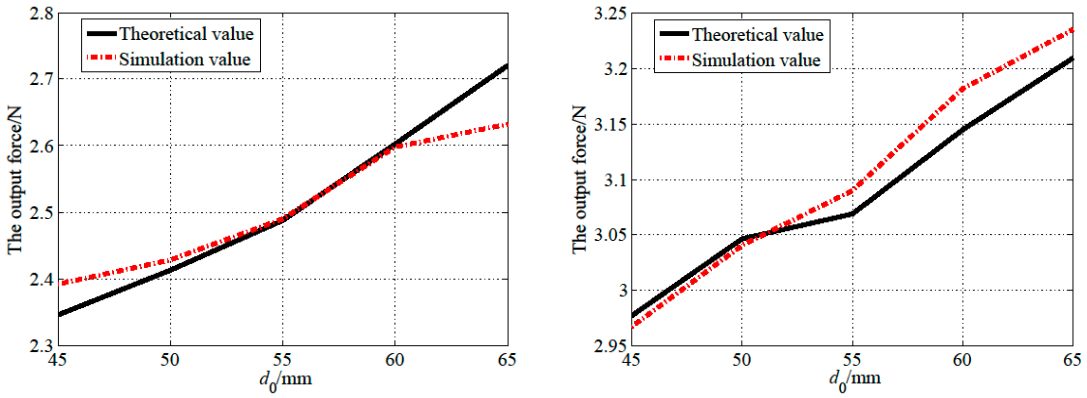

Figure 11. Grasping force simulation results in two modes with a torque of 171 N·mm. (**a**) Two-point clamping mode. (**b**) Envelope clamping mode.

In order to compare the response time when the output force is stable for the cable-driven rigid flexible combination manipulator in different clamping modes, a simulation analysis is carried out on the variation of the output force with time. The cable-driven torque is 171 N·mm, and the results are shown in Figure 12. In the two modes, the stable response time of the output force is 2 s. That is, the oscillation is obvious within 0–2 s, and the output force generally tends to be stable after 2 s. However, the stability of the output force after 2 s in envelope grasping mode is better than that in two-point clamping mode. The reason for this may be that envelope grasping occurs through surface contact, the contact force is evenly distributed, and the grasping stability is greater.

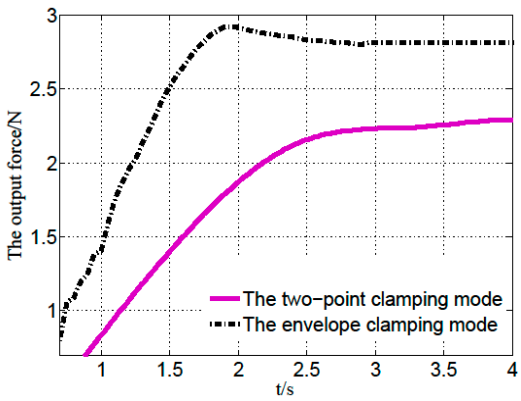

Figure 12. Time domain analysis diagram of the output force in different modes.

4. Sensitivity Analysis

To determine the relationship between the manipulator grasping performance and the variation in the design parameters, a sensitivity analysis of the manipulator design parameters was carried out. The sensitivity analysis was divided into global sensitivity analysis and local sensitivity analysis. Due to the complex structure and many dimensional design variables of the cable-driven rigid–flexible combined manipulator designed in this paper, it is difficult to obtain the sensitivity of the design parameters by using the direct derivation method in the local sensitivity analysis. The global sensitivity analysis method can be used to test the total influence of the common changes of multiple design variables on the model output, which is suitable for systems with strong nonlinearity or nonmonotonicity [26]. In this section, the global sensitivity analysis method based on variance is used to analyze the dimensional parameter sensitivity of the cable-driven rigid–flexible combined manipulator. In this method, the model is decomposed into independent single parameters, the functions of the parameters are combined with each other, and the

sensitivity of the parameters is analyzed by calculating the influence of the variance of a single design variable or variable set on the total output variance [27].

4.1. Sensitivity of the Design Parameters

The stable grasping performance of the cable-driven rigid–flexible combined manipulator was measured in terms of the output force. Parameters that affect grasping performance were determined through force analysis using grasping tests. Based on the performance test analysis results, sensitivity analysis modeling was conducted to determine the influence of each possible parameter on the grasping performance of the cable-driven rigid–flexible combined manipulator. Then, the Monte Carlo method was used to calculate the variance in a specific probability distribution, resulting in design variables with low parameter sensitivity, which were set as constant values to simplify complex multi-parameter optimization schemes. Parameters with high sensitivity were selected for multi-objective optimization analysis of the manipulator to obtain the maximum contact force of the multimode manipulator.

According to force analysis and modeling, the parameters $l_1, l_2, l_4, d, d_1, d_2, t, w$ affect the output force of the manipulator. Therefore, the above parameters were set as the design variables of sensitivity analysis and recorded as vectors $\omega = [l_1, l_2, l_4, d, d_1, d_2, t, w]$.

The output force of manipulator is a function of the design variable ω, i.e., $\boldsymbol{F}_{\text{out}} = f(\omega)$. It is assumed that the elements in the vector are independent of each other. The vector ω is normalized to $\boldsymbol{a} = (a_1, a_2, \cdots, a_\lambda)$. Thus, the following expression can be obtained:

$$a_i = \frac{\omega_i - \omega_{i\min}}{\omega_{i\max} - \omega_{i\min}}, i = 1, 2, \cdots, \lambda \tag{29}$$

The purpose of normalization is so that each parameter index can be comprehensively compared in the same order of magnitude. Furthermore, the model $\boldsymbol{F}_{\text{out}} = f(a)$ is divided as follows:

$$f(a) = f_0 + f_i(a_i) + f_j(a_j) + f_{i,j}(a_i, a_j) \tag{30}$$

where f_0 is independent of vector $\boldsymbol{a}$, and the split function is only related to the corresponding independent variable.

The sensitivity of the variable relative to the output force of the manipulator can be expressed as:

$$S_{ai} = \frac{V_{ai}(\boldsymbol{F}_{\text{out}})}{V(\boldsymbol{F}_{\text{out}})} \tag{31}$$

where the total variance $V(\boldsymbol{F}_{\text{out}})$ represents the degree to which the output force function $\boldsymbol{F}_{\text{out}}$ is affected by the output force model when all parameters in the normalized sensitivity analysis vector $\boldsymbol{a}$ change, and the biased variance $V_{ai}(\boldsymbol{F}_{\text{out}})$ represents the change in function $\boldsymbol{F}_{\text{out}}$ when only a single variable a_i is considered.

According to the relationship between the variance and mathematical expectation, the following expression can be obtained:

$$\begin{aligned} V(\boldsymbol{F}_{\text{out}}) &= \text{Ex}\left(\boldsymbol{F}_{\text{out}}^2\right) - \left(\text{Ex}(\boldsymbol{F}_{\text{out}})\right)^2 \\ &= \int_0^1 \int_0^1 \cdots \int_0^1 \boldsymbol{F}_{\text{out}}^2 \text{d}a_1 \text{d}a_1 \ldots \text{d}a_\lambda - \left(\int_0^1 \int_0^1 \cdots \int_0^1 \boldsymbol{F}_{\text{out}} \text{d}a_1 \text{d}a_1 \ldots \text{d}a_\lambda\right)^2 \end{aligned} \tag{32}$$

Therefore, the deviation in output force relative to the design parameters is expressed as:

$$V_{\text{ai}}(\boldsymbol{F}_{\text{out}}) = \int_0^1 f_{a_i}^2 \text{d}a_i (i = 1, 2, \ldots, \lambda) \tag{33}$$

Due to the complex structure of the output force model, the integral calculation of Equations (32) and (33) is difficult to solve analytically. Because the design variable ω obeys the uniform distribution condition within its value range, we can obtain vector $\boldsymbol{a}$ through normalization, which meets the conditions of Monte Carlo statistical sampling to

calculate the probability problem of complex objects. Therefore, the Monte Carlo method was proposed to calculate the total variance and deviation. The flowchart for calculating the total variance and deviation based on the Monte Carlo method is shown in Figure 13.

The sensitivity of the design parameters was calculated using an example. The parameters are shown in Table 1. The sampling base was set to N = 1000 for the calculation, and the total variance and the partial square difference of each single variable were calculated in two-point clamping and envelope grasping modes, respectively. By substituting these values into Equation (33), the sensitivities of different parameters relative to the output force function in different modes were obtained, as shown in Figure 14. Figure 14 shows that in two-point clamping and envelope grasping modes, the sensitivity of the length of the flexible beam is 0.7404 and 0.7265, respectively, which is much greater than that of the other design variables, so the function $\boldsymbol{F}_{\text{out}}$ is most affected by the length of the flexible beam.

Table 1. Range of input variables.

Design Variable ω	Range (mm)	Design Variable ω	Range (mm)
l_1	(56–65)	d_1	(5–8)
l_2	(27–40)	d_2	(20–24)
l_4	(68–78)	t	(1–2)
d	(16–20)	w	(7–8)

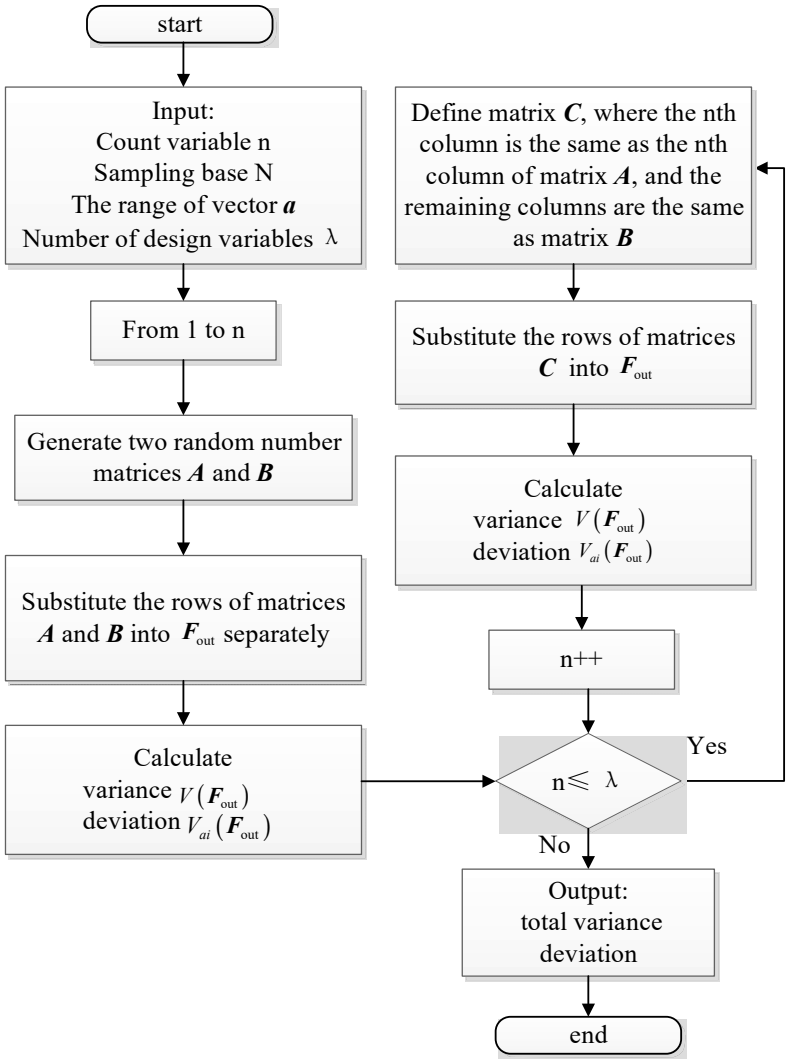

Figure 13. Flowchart of calculation for total variance and deviation using the Monte Carlo method.

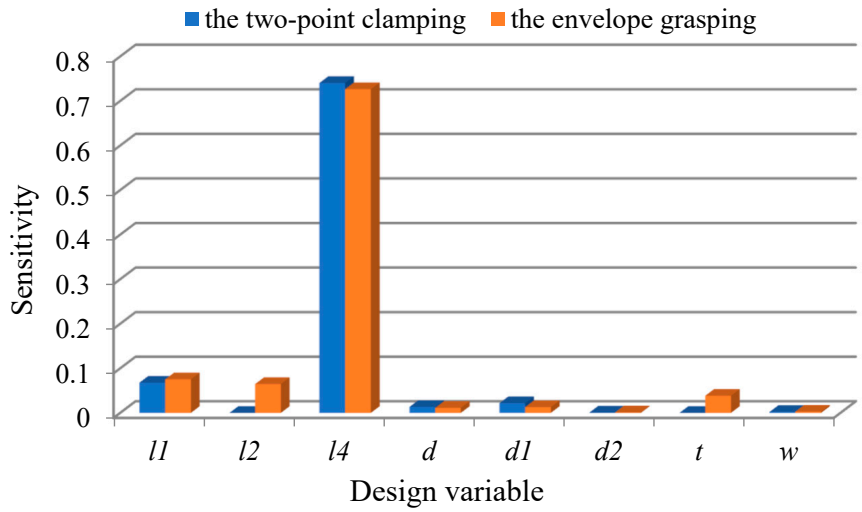

Figure 14. Sensitivity of each input variable to the output force.

4.2. Simulation Analysis of the Sensitivity

To verify the effectiveness of the sensitivity, seven groups of numerical examples were selected for simulation. The value of one design variable was changed in turn on the basis of the control variable method, and the values of the other design variables remained unchanged. For the simulation software, the same boundary conditions were set, and the effectiveness of the sensitivity was verified by calculating and comparing the change rate of the output force in each case. Table 2 shows the specific size parameters of each calculation example.

Table 2. Dimension parameters of each case in the sensitivity simulation.

Numerical Example	l_1	l_2	l_4	d	d_1	d_2	t	w
Reference group	60.5	33.5	73	18	6.5	22	1.5	7.5
First group	63.5	33.5	73	18	6.5	22	1.5	7.5
Second group	60.5	35.2	73	18	6.5	22	1.5	7.5
Third group	60.5	33.5	76.7	18	6.5	22	1.5	7.5
Fourth group	60.5	33.5	73	18.9	6.5	22	1.5	7.5
Fifth group	60.5	33.5	73	18	6.8	22	1.5	7.5
Sixth group	60.5	33.5	73	18	6.5	23.1	1.5	7.5
Seventh group	60.5	33.5	73	18	6.5	22	1.6	7.5
Eighth group	60.5	33.5	73	18	6.5	22	1.5	7.9

It is assumed that the input cable tension is 20 N and the grasped target is a cylinder with a radius of 50 mm. The simulation results are shown in Figure 15. From the relationship between the input force and the output force in the figure, it can be seen that in the two clamping modes, when the size of the flexible beam is increased, the output force changes the most, that is, the size sensitivity of the flexible beam is the strongest. The changes in other parameters have little effect on the output force of the manipulator, which can almost be ignored. Therefore, the sensitivity analysis of the design parameters was effective.

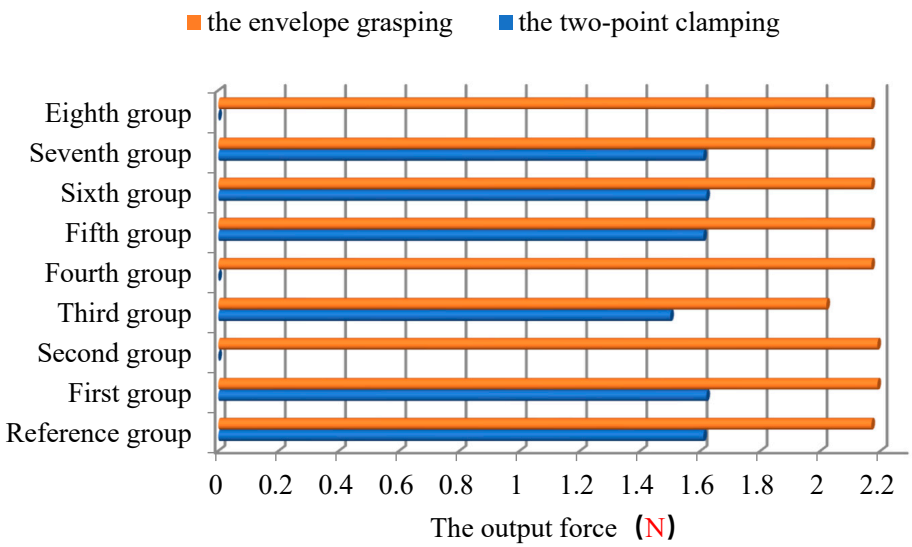

Figure 15. Relationship between the design parameters and output force in two modes.

5. Grasping Performance Experimental Verification

To verify the grasping performance of the manipulator, a test prototype of the cable-driven rigid–flexible combined manipulator was designed and analyzed. The main components of the test platform include a cable-driven rigid–flexible manipulator, laser displacement sensor, pressure sensor (DYHW-108, DAYSEN-SOR, Guangzhou, China), dynamometer (DS2-500N, PUYAN, Guangzhou, China), and digital display, as shown in Figure 16. An output force stability test was carried out on the manipulator prototype, and the theoretical and experimental results were compared to verify the validity of the static model for the two grasping modes.

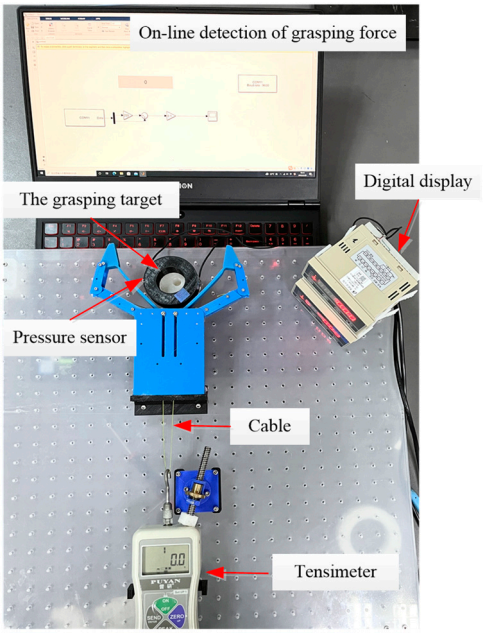

Figure 16. Test prototype of the cable-driven rigid–flexible combined manipulator.

The rigid grasping mechanism and the grasped targets were fabricated using 3D printing technology, and the flexible grasping mechanism was fabricated using lamination processing technology. The dynamometer was used to measure the cable force, and the pressure sensor was attached to the left and right sides of the grasped object to measure the output force. Two types of comparative tests were set up in the test. One involved changing

the cable force and measuring the change in the output force while keeping the radius of the grasped targets unchanged. The other involved keeping the cable force unchanged and changing the radius of the grasped target to measure the change in the output force. Five groups were set up for each type of experiment, and six repeated measurements were performed in each group to obtain the average value.

5.1. Clamping Test in Two-Point Clamping Mode

In two-point clamping mode, when the grasped target radius was 55 mm, the change in the output force was calculated as shown in Figure 17a. It can be seen from the figure that the change trends of the experimental, theoretical, and simulation values in two-point clamping mode are similar, and the output force increases linearly with increasing cable force. When the cable force was less than 30 N, the simulation value and experimental value increased more than the theoretical value. When the cable force was greater than 30 N, the increase in the experimental value was smaller than that in the theoretical value. This shows that as the cable force increases, the friction between the cable and the pulley also increases, resulting in loss. The maximum relative error between the experimental value and the theoretical value was 6.27%, which is within the allowable range for engineering applications.

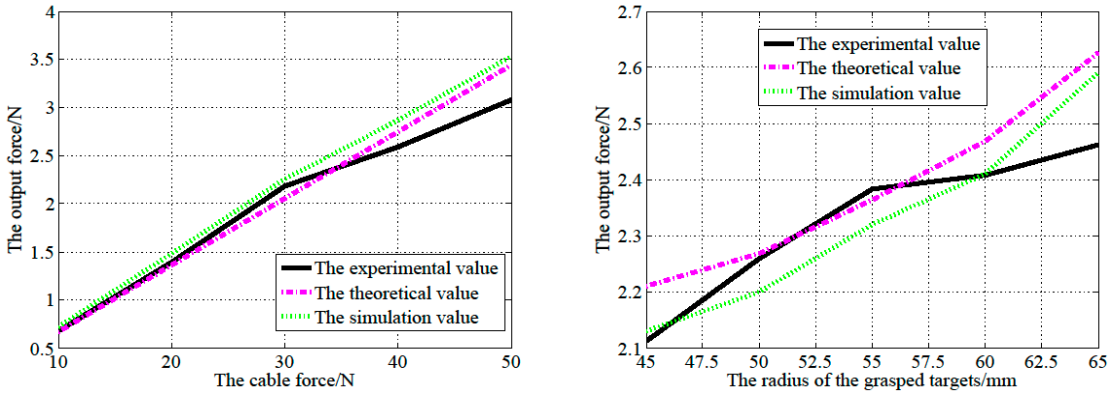

(**a**) (**b**)

Figure 17. Change in output force in two-point clamping mode. (**a**) The grasped target radius is a constant. (**b**) The cable force is a constant.

When the cable force was 30 N, the change in output force was calculated as shown in Figure 17b. In two-point clamping mode, the variation trends of the experimental, theoretical, and simulation values were similar, and the output force increased with increasing grasped target radius. When the grasped target radius was less than 55 mm, the error between the experimental value and the theoretical value gradually decreased. When the grasped target radius was greater than 55 mm, the error between the experimental value and the theoretical value gradually increased. Because the radius of the grasped target was too large, the contact point between the manipulator and the grasped target fluctuated and evolved from two-point clamping to envelope grasping, and the force of the grasped target was unstable, which led to an increase in error.

To verify the grasp stability of the manipulator in two-point clamping mode, a stability test of the output force was carried out. The results are shown in Figure 18. It can be seen from the figure that the output force increases rapidly within 0–2.5 s and is in a stable output state after 2.5 s, indicating that the response time of the output force in the two-point clamping mode is 2.5 s. The maximum error between the experimental value and the simulation value was 5.84%, which is within the allowable range for engineering applications.

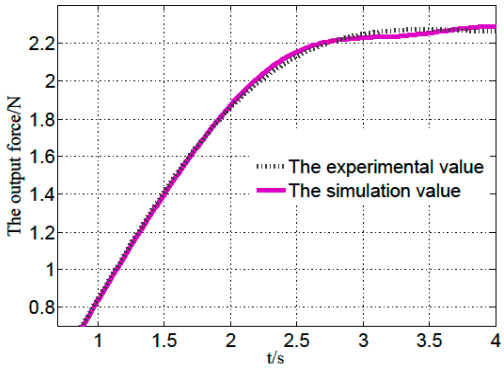

Figure 18. Stability of the output force in two-point clamping mode.

5.2. Grasping Test in Envelope Grasping Mode

In envelope grasping mode, when the grasped target radius was 55 mm, the change in output force was calculated as shown in Figure 19a. It can be seen from the figure that the change trends of the experimental, theoretical, and simulation values in envelope grasping mode are similar, and the output force increases linearly with increasing cable force. The experimental value was always smaller than the theoretical value, which may have been due to friction during the test. The maximum relative error between the experimental value and the theoretical value was 5.37%, which is within the allowable range for engineering applications.

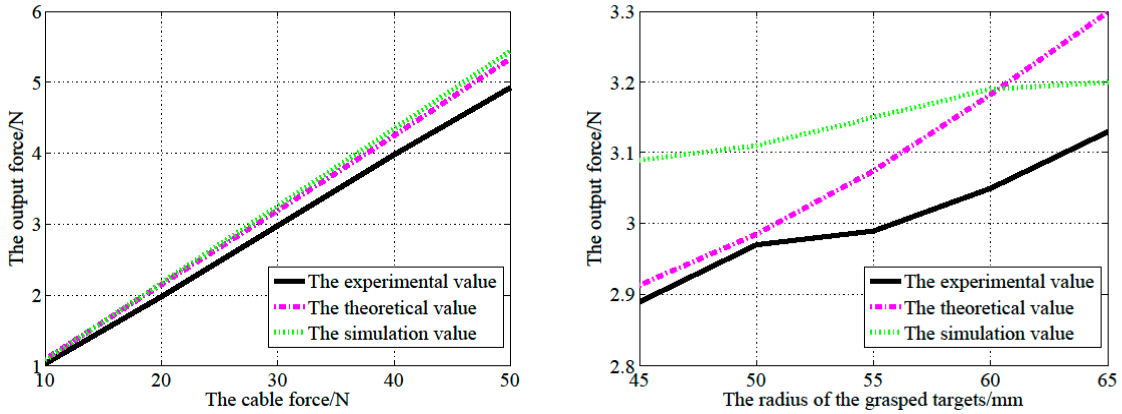

(**a**) (**b**)

Figure 19. Change in output force in envelope grasping mode. (**a**) The grasped target radius is a constant. (**b**) The cable force is a constant.

When the cable force was 30 N, the change in output force was calculated as shown in Figure 19b. In envelope grasping mode, the experimental, theoretical, and simulation values had similar changing trends, and the output force increased with increasing grasped target radius. The error between the experimental value and the theoretical value decreased gradually when the grasped target radius was less than 50 mm. When the grasped target radius was greater than 50 mm, the error between the experimental value and the theoretical value gradually increased. It may be that as the radius of the grasped target increases, the contact surface between the flexible beam and the grasped target increases, and the cumulative error of the output force increases.

To verify the grasping stability of the manipulator in envelope grasping mode, a stability test of the output force was carried out. The results are shown in Figure 20. It can be seen from the figure that the response time of the output force in envelope grasping mode is the same as that in two-point clamping mode, which is 2.5 s, and the output force is in a stable state after 2.5 s. The maximum error between the experimental value

and the simulated value was 2.27%, which is within the allowable range for engineering applications.

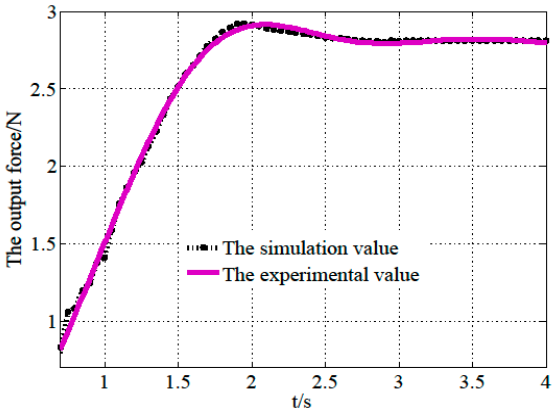

Figure 20. Stability of the output force in envelope grasping mode.

5.3. Fruit Grasping Test

To verify the antibreakage grasping performance of the cable-driven rigid–flexible combined manipulator, grasping experiments were carried out on common fruits, as shown in Figure 21. The grasped targets were a grape, banana, brin, plum, orange, pear, mango, and peach, which have different shapes and sizes. In the fruit grasp tests, the gripper was attached to a robot arm. This study controlled the cable's retraction and release motion through the forward and reverse rotation of the motor, achieving the target's grasping and releasing. Since the grasp tests' purpose was to prove that the cable-driven rigid–flexible combined manipulator could achieve two-point clamping and enveloping grasping of fruits, this study artificially adjusted the positions of fruits during the test. There is a pre-contact process between the cable-driven rigid–flexible combined manipulator and the fruits, rather than automatically grasping through the visual system as a fruit picking robot.

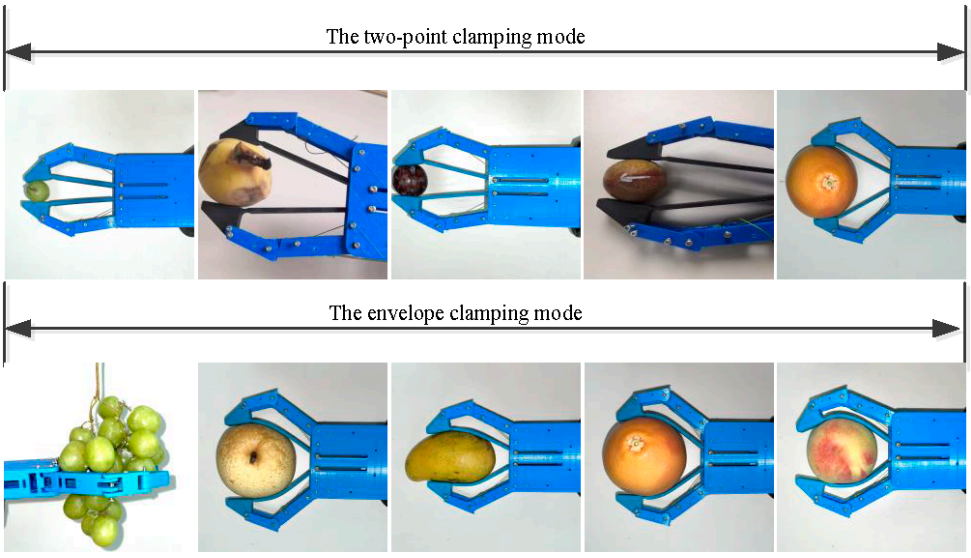

Figure 21. Grasping experiment with common fruits.

The grasping test showed that the grasping mode gradually changed from two-point clamping to envelope grasping with increasing size. It can be concluded that there is a certain relationship between the grasped target size and the grasping mode. During enveloping clamping, the flexible beam plays a certain role in protecting the fruit. The approximate range of two-point clamping and envelope grasping was obtained through

experiments, as shown in Table 3. It is worth noting that when the two-point clamping and envelope grasping ranges overlap, envelope grasping is more stable. When the envelope grasping range is exceeded, the manipulator automatically changes back to two-point clamping mode, and the critical value is approximately 110 mm.

Table 3. Grasping range of the two grasping modes.

Grasp Mode	Range (mm)
Two-point clamping	0.1~150
Envelope grasping	30~110

5.4. Comparative Experiments

In order to highlight the advantages of the cable-driven manipulator, a comparative test was conducted. The same grasping task was performed using a link-driven compliant manipulator independently developed at our laboratory [28]. The weight of the cable-drive manipulator is 173 g, and the weight of the link-driven compliant manipulator is 1122 g. The cable-driven manipulator has absolute advantages in weight. The sizes of the grasped targets are shown in Table 4. It can be seen from Figure 22 that the cable-driven manipulator is smaller than the link-driven compliant manipulator in size. The maximum opening size of the cable-driven manipulator is 133 mm, while the maximum opening size of the link-driven compliant manipulator is 120 mm.

Table 4. Size of the grasped targets.

Grasping Target	Size (mm)
The thickness of a rectangular box	28.80
Cylindrical bottle	35.50
Banana	16.50
Solid glue	12.10
Black cylindrical bottle	20.30

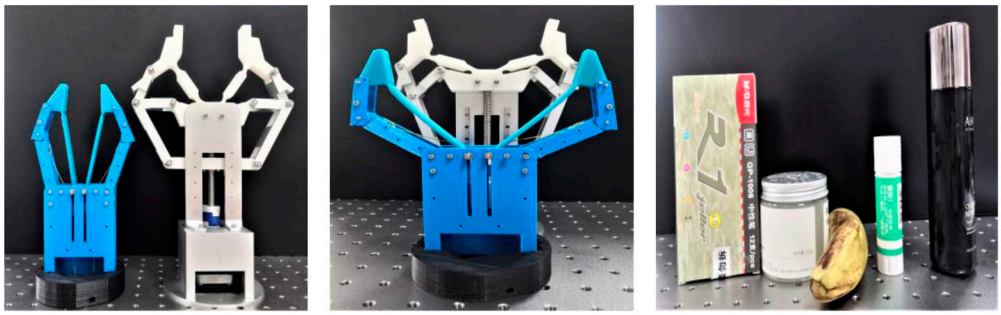

(a) (b) (c)

Figure 22. Cable-driven manipulator, link-driven compliant manipulator, and grasping targets. (**a**) Original state; (**b**) Maximum opening state; (**c**) Grasping target.

To compare the stable grasping performance between the cable-driven manipulator and link-driven compliant manipulator, the grasping tests were performed on grasping targets of different sizes, as shown in Figure 23. The changes in input force and grasping force are shown in Figure 24. The maximum output efficiency of the cable-driven manipulator was 64.29%, and the minimum output efficiency was 52.38%. The maximum output efficiency of the link-driven compliant manipulator was 50%, and the minimum output efficiency was 45.83%. To grasp the same targets, the cable-driven manipulator requires greater input force to achieve stable grasping, and its output efficiency is higher.

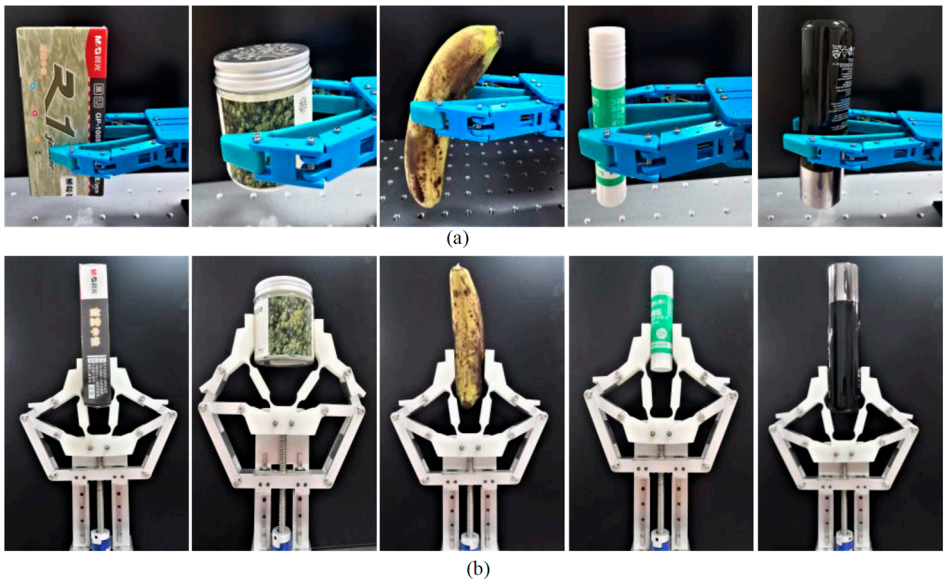

Figure 23. Grasping experiment with two types of manipulator. (**a**) Grasping experiment with cable-driven gripper; (**b**) Grasping experiment with link-driven compliant gripper.

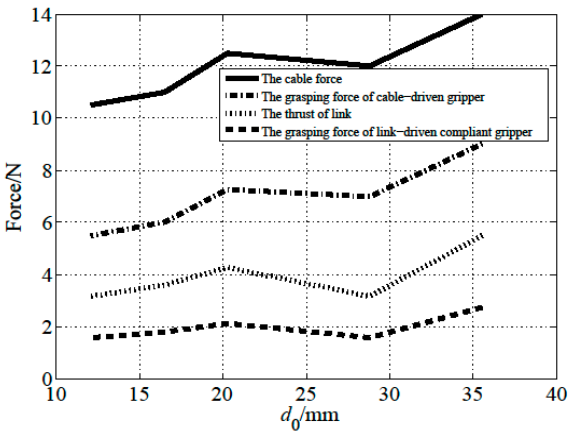

Figure 24. Comparison of grasping force between two types of manipulator.

With reference to the above grasping test, compared to the link-driven compliant manipulator, the adaptive cable-driven manipulator has several remarkable advantages: (1) the size is more compact, and it is more conducive to the task of limited workspace, such as long-distance transmission in a small space; (2) the design is relatively simple, easy to manufacture, and reconfigurable; (3) it is more lightweight, has smaller motion inertia, and is more suitable for high-speed operating occasions; (4) it can be modularized with 3D printing, resulting in lower cost; (5) it can produce a large output force and is highly efficient. All of these advantages in the adaptive cable-driven manipulator have contributed to some practical applications, such as limb rehabilitation training, fruit and vegetable picking, surgical operation, high-speed grasping, and so on.

6. Discussion

A comparison between the results obtained using the analytical model and a numerical implementation is presented in Section 3. There are some relative errors. The reasons for the errors may include neglecting the friction of the cable-driven systems and the elastic deformation of twisted springs and flexible materials. In future research work, it is necessary to consider establishing a more accurate static model.

This study analyzed the sensitivity of design parameters in Section 4. By comparing the theoretical sensitivity calculation results in Figure 14 with the simulation results in

Figure 15, it can be seen that the cable-driven rigid–flexible combined manipulator is most sensitive to changes in the size of the flexible beam.

This study conducted experiments under different grasping modes, fruit grasping experiments, and comparative comparison tests with a link-driven compliant manipulator, as shown in Section 5. Although there are errors in the theoretical model and experimental results, they are within the acceptable range of engineering. According to the experimental results, the cable-driven rigid–flexible manipulator can smoothly achieve automatic switching between two grasping modes and has certain advantages in lightweight and output efficiency.

Through the above theoretical analysis and experimental verification, it can be concluded that the novelty of this article is the design of a cable-driven rigid–flexible manipulator with a cable drive system and compliant hinge structure that can automatically switch between two-point clamping and envelope clamping modes, solving the problem of the traditional manipulator's difficulty to stably grip special-shaped objects with complex contours, and improving the self-adaptability and protective grasping ability of the manipulator.

7. Conclusions

The structures of the cable-driven unit and compliant unit of the cable-driven rigid–flexible combined manipulator were constructed in this research to examine the adaptability and compliance of the manipulator, and the Monte Carlo method was used to analyze the global sensitivity of the design parameters. The cable-driven rigid–flexible combined manipulator's grasping model was developed by analyzing the finger force in two-point clamping mode and envelope grasping mode. Numerical simulations and prototype testing were carried out to confirm the cable-driven rigid–flexible combined manipulator's grasping capabilities. The test results demonstrated that the cable-driven system's flexibility enables the manipulator's adaptability, the compliant unit's compliance enables the manipulator's compliance, and the cable-driven rigid–flexible combined manipulator's good adaptability and compliance enable the adaptive and stable grasping of delicate and uniquely shaped parts.

Despite this research realizing automatic switching between two-point clamping and envelope grasping, the cable-driven manipulator does not have the ability to perceive and is unable to perform dexterous operations. The cable-driven manipulator's grasping control will undoubtedly be major area of research in the future. A grasping control for a robotic hand–eye system was developed in [29], which implemented the task of grasping an object. It is worthwhile to learn manipulation based on sensory–motor fusion. The cable-driven manipulator is a strong nonlinear coupling mechanism. A previous study [30] showed an example of grasping planning in which an autonomous motion planning method considering multiple conflicting performance metrics for a class of robots was designed, and a method of improving robustness and adaptability can be seen in [31].

The cable-driven rigid–flexible manipulator designed in this research, which is capable of actively transitioning between clamping and grasping, can be widely applied in fields such as agricultural picking, food sorting, fragile product grabbing, and underwater biological fishing. To achieve commercial applications in these fields, it is also necessary to improve the intelligent perception ability and high-precision robust control performance of the cable-driven rigid–flexible manipulator. In short, there are still many works worthy of in-depth research on the cable-driven manipulator.

Author Contributions: Conceptualization, H.W. and J.L.; methodology, H.W., Q.L. and L.L.; software, J.L. and W.C.; validation, H.W., J.L. and C.L.; formal analysis, H.W.; investigation, H.W.; resources, Q.L.; data curation, J.L. and C.L.; writing—original draft preparation, H.W.; writing—review and editing, J.L., W.C. and L.L.; supervision, Q.L.; project administration, H.W.; funding acquisition, H.W., Q.L., W.C. and L.L. All authors have read and agreed to the published version of the manuscript.

Funding: The authors gratefully acknowledge the National Natural Science Foundation of China (Grant Nos. 52205254), the financial support of the Natural Science Foundation of Guangdong Province of China (grants nos. 2020A1515111056, 2020B1515120070, and 2020B1515120050), and the Research Projects of Universities Guangdong Province (grant nos. 2021KTSCX118 and 2020KCXTD015). The authors are grateful for their generous financial assistance.

Data Availability Statement: The data used to support the findings of the cable-driven rigid–flexible combined manipulator are available from the corresponding author upon request.

Acknowledgments: The authors are grateful to the editor and anonymous reviewers for their constructive comments and helpful suggestions, which greatly improved the quality of this article.

Conflicts of Interest: The authors declare that there are no conflict of interest regarding the publication of this paper.

References

1. Cai, S.B.; Tao, Z.C.; Wan, W.W.; Yu, H.Y.; Bao, G.J. Multi-fingered dexterous hands: From simplicity to complexity and simplifying complex applications. *J. Mech. Eng.* **2021**, *57*, 1–14.
2. Xiong, Y.; Peng, C.; Grimstad, L.; From, P.J.; Isler, V. Development and field evaluation of a strawberry harvesting robot with a cable-driven gripper. *Comput. Electron. Agric.* **2019**, *157*, 392–402. [CrossRef]
3. Klausen, K.; Meissen, C.; Fossen, T.I.; Arcak, M.; Johansen, T.A. Cooperative control for multirotors transporting an unknown suspended load under environmental disturbances. *IEEE Trans. Control Syst. Technol.* **2020**, *28*, 653–660. [CrossRef]
4. Shirani, B.; Najafi, M.; Izadi, I. Cooperative load transportation using multiple UAVs. *Aerosp. Sci. Technol.* **2019**, *84*, 158–169. [CrossRef]
5. Tang, S.; Wuest, V.; Kumar, V. Aggressive flight with suspended payloads using vision-based control. *IEEE Robot. Autom. Lett.* **2018**, *3*, 1152–1159. [CrossRef]
6. Klausen, K.; Fossen, T.I.; Johansen, T.A. Autonomous recovery of a fixed-wing UAV using a net suspended by two multirotor UAVs. *J. Field Robot.* **2018**, *35*, 717–731. [CrossRef]
7. Wang, W.; Chen, J.Y.; Ding, Q.; Zhang, J.J.; Liu, J.T. Improving walking economy with an ankle exoskeleton prior to human-in-the-loop optimization. *Front. Neuro Robot.* **2021**, *15*, 797147. [CrossRef]
8. Wei, H.L.; Qiu, Y.Y.; Sheng, Y. On the cable pseudo-drag problem of cable-driven parallel camera robots at high speeds. *Robotica* **2019**, *37*, 1695–1709. [CrossRef]
9. Kashef, S.R.; Amini, S.; Akbarzadeh, A. Robotic hand: A review on linkage-driven finger mechanisms of prosthetic hands and evaluation of the performance criteria. *Mech. Mach. Theory* **2020**, *145*, 103677. [CrossRef]
10. Babin, V.; Gosselin, C. Mechanisms for robotic grasping and manipulation. *Annu. Rev. Control Robot. Auton. Syst.* **2021**, *4*, 573–593. [CrossRef]
11. Zhang, Z.K.; Shao, Z.F.; You, Z.; Tang, X.Q.; Zi, B.; Yang, G.L.; Gosselin, C.; Caro, S. State-of-the-art on theories and applications of cable-driven parallel robots. *Front. Mech. Eng.* **2022**, *17*, 37. [CrossRef]
12. Ma, R.R.; Spiers, A.; Dollar, A.M. M^2 Gripper: Extending the dexterity of a simple, underactuated gripper. In Proceedings of the ASME/IFToMM International Conference on Reconfigurable Mechanisms and Robots, Beijing, China, 20–22 July 2015; pp. 795–805.
13. Bircher, W.G.; Dollar, A.M.; Rojas, N. A two-fingered robot gripper with large object reorientation range. In Proceedings of the 2017 IEEE International Conference on Robotics and Automation (ICRA), Singapore, 29 May–3 June 2017; pp. 3453–3460.
14. Firouzeh, A.; Paik, J. Grasp mode and compliance control of an underactuated origami gripper using adjustable stiffness joints. *IEEE/ASME Trans. Mechatron.* **2017**, *22*, 2165–2173. [CrossRef]
15. Dong, H.X.; Asadi, E.; Qiu, C.; Dai, J.S.; Chen, I.M. Grasp analysis and optimal design of robotic fingertip for two tendon-driven fingers. *Mech. Mach. Theory* **2018**, *130*, 447–462. [CrossRef]
16. Leddy, M.T.; Dollar, A.M. Stability optimization of two-fingered anthropomorphic hands for precision grasping with a single actuator. In Proceedings of the 2019 International Conference on Robotics and Automation, Montreal, QC, Canada, 20–24 May 2019; pp. 451–457.
17. Kim, Y.J.; Song, H.; Maeng, C.Y. BLT gripper: An adaptive gripper with active transition capability between precise pinch and compliant grasp. *IEEE Robot. Autom. Lett.* **2020**, *5*, 5518–5525. [CrossRef]
18. Hussain, I.; Al-Ketan, O.; Renda, F.; Malvezzi, M.; Prattichizzo, D.; Seneviratne, L.; Abu Al-Rub, R.K.; Gan, D.M. Design and prototyping soft-rigid tendon-driven modular grippers using interpenetrating phase composites materials. *Int. J. Robot. Res.* **2020**, *39*, 1635–1646. [CrossRef]
19. Min, S.; Yi, S. Development of cable-driven anthropomorphic robot hand. *IEEE Robot. Autom. Lett.* **2021**, *6*, 1176–1183. [CrossRef]
20. Zhang, P.; Chen, W.C.; Tang, B. From two-dimensional to three-dimensional: Diversified bending modality of a cable-driven actuator and its grasping characteristics. *Soft Robot.* **2022**, *9*, 1154–1166. [CrossRef]
21. Xiong, P.W.; Tong, X.B.; Song, A.G.; Liu, P.X. Robotic multifinger grasping state recognition based on adaptive multikernel dictionary learning. *IEEE Trans. Instrum. Meas.* **2022**, *71*, 2511014. [CrossRef]

22. Zhang, H.; Peeters, J.; Demeester, E.; Kellens, K. Deep learning reactive robotic grasping with a versatile vacuum gripper. *IEEE Trans. Robot.* **2023**, *39*, 1244–1259. [CrossRef]
23. Trease, B.P.; Moon, Y.M.; Kota, S. Design of large-displacement compliant joints. *J. Mech. Des.* **2005**, *127*, 788–798. [CrossRef]
24. Lobontiu, N. *Compliant Mechanisms: Design of Flexure Hinges*; CRC Press: New York, NY, USA, 2003.
25. Lobontiu, N.; Paine, J.S.N.; Garcia, E.; Goldfard, M. Design of symmetric conic-section flexure hinges based on closed-form compliance equations. *Mech. Mach. Theory* **2002**, *37*, 477–498. [CrossRef]
26. Yin, J.J.; Chang, F.; Li, S.L.; Yang, Z.; Shi, X.P. Analysis of parameter sensitivity on damage tolerance design of overall beam based on Sobol method. *J. Air Force Eng. Univ. (Nat. Sci. Ed.)* **2013**, *14*, 9–12.
27. Chen, W.L.; He, X.L.; Lu, Q.H.; Zhang, Y.Z.; Qiao, J.; Wei, H.L. Design and analysis of the compliant orthogonal two-stage leverage displacement amplification mechanism. *Comput. Integr. Manuf. Syst.* **2023**, *29*, 740–751.
28. Chen, W.L.; Feng, Z.H.; Lu, Q.H.; Huang, M.X.; Zhang, P.X.; Zhang, Q.H. Design, analysis and experimental test of a multi-mode rigid-flexible underactuated grasping mechanism. *Robot* **2022**, *44*, 139–152.
29. Hu, Y.B.; Li, Z.J.; Li, G.L.; Yuan, P.J.; Yang, C.G.; Song, R. Development of sensory-motor fusion-based manipulation and grasping control for a robotic hand-eye system. *IEEE Trans. Syst. Man Cybern. Syst.* **2017**, *47*, 1169–1180. [CrossRef]
30. Hu, Y.B.; Li, Z.J.; Yen, G.G. A knee-guided evolutionary computation design for motor performance limitations of a class of robot with strong nonlinear dynamic coupling. *IEEE Trans. Syst. Man Cybern. Syst.* **2023**, *53*, 4429–4441. [CrossRef]
31. Hu, Y.B.; Chen, G.; Li, Z.J.; Knoll, A. Robot Policy Improvement with Natural Evolution Strategies for Stable Nonlinear Dynamical System. *IEEE Trans. Cybern.* **2023**, *53*, 4002–4014. [CrossRef]

Disclaimer/Publisher's Note: The statements, opinions and data contained in all publications are solely those of the individual author(s) and contributor(s) and not of MDPI and/or the editor(s). MDPI and/or the editor(s) disclaim responsibility for any injury to people or property resulting from any ideas, methods, instructions or products referred to in the content.